Supporting information

The superiority of Pd^{2+} in CO_2 hydrogenation to formic acid

Yanyan Wang,[a,b] Minghua Dong,[b,c] Shaopeng Li,[b,c] Bingfeng Chen,[b] Huizhen Liu*[b,c] and Buxing Han*[b,c]

[a] *National Narcotics Laboratory Beijing Regional Center, Beijing 100164, P. R. China.*

[b] *Beijing National Laboratory for Molecular Sciences, Key Laboratory of Colloid and Interface and Thermodynamics, CAS Research/Education Center for Excellence in Molecular Sciences, Institute of Chemistry, Chinese Academy of Sciences, Beijing 100190, P. R. China. Tel./fax: +86 10 6256282.*

[c] *School of Chemical Science, University of Chinese Academy of Sciences, Beijing 100049, China; E-mail: liuhz@iccas.ac.cn; hanbx@iccas.ac.cn.*

1. Experimental

Materials

Palladium acetylacetone ($Pd(acac)_2$) and acetylacetone vanadium oxide ($VO(acac)_2$) were obtained from Alfa. The activated carbon was purchased from Fujian Xinsen Chemical Industry Co. Ltd., sodium carbonate, sodium bicarbonate, sodium hydroxide, potassium bicarbonate and acetone were provided by Sinopharm Chemical Reagent Co., Ltd. Triethylamine, ammonium bicarbonate and cesium carbonate were supplied by innochem. Commercial SBA15, SiO_2, a-TiO_2, P25 and disordered mesoporous carbon (DMC) were provided by the Acros. CO_2 (99.99%) and H_2 (99.99%) were provided by Beijing Analytical Instrument Company. All solvents and chemicals were used as received without further purification.

Catalyst preparation

Preparation of the Pd-V/AC-air: palladium acetylacetone ($Pd(acac)_2$, 0.06 mmol) and acetylacetone vanadium oxide ($VO(acac)_2$, 0.06 mmol) were dissolved in 60 mL acetone, after complete dissolution, 0.6 g activated carbon (AC) was impregnated into the prepared solution and stirred for 2 h. Next, the solvent was removed via the vacuum rotary evaporation. Finally, the obtained powder was calcined in air at 300°C with a temperature rate of 5°C/min.

Preparation of the Pd/AC-air was similar except that the addition of vanadium precursor is not included.

Preparation of the Pd-V/a-TiO_2-air, Pd-V/P25-air, Pd-V/SiO_2-air, Pd-V/SBA15-air and Pd-V/disordered mesoporous carbon-air (Pd-V/DMC-air) was similar except the amount of the precursor and the support, the ratio of Pd/V is also 1.

Preparation of the Pd-V/AC-H_2: palladium acetylacetone ($Pd(acac)_2$, 0.06 mmol) and acetylacetone vanadium oxide ($VO(acac)_2$, 0.06 mmol) were dissolved in 60 mL acetone, after complete dissolution, 0.6 g activated carbon (AC) was impregnated into the prepared solution and stirred for 30 min. Next, the solvent was removed via the vacuum rotary evaporation. Finally, the obtained powder was reduced in10%H_2/Ar at 300°C with a temperature rate of 5°C/min.

Preparation of the Pd/AC-H_2 was similar except that the addition of vanadium precursor is not included.

Preparation of the Pd-V/AC-H_2-air: the Pd-V/AC-H_2 was calcined in air at 300°C with a temperature rate of 5°C/min.

Catalyst characterization

The prepared catalyst was characterized by transmission electron microscopy (TEM), X-ray diffraction (XRD), X-ray photoelectron spectroscopy (XPS), inductively coupled plasma-atomic emission spectroscopy (ICP-AES) and X-ray absorption spectroscopy (XAS) techniques. The TEM images were obtained through a Hitachi-7700 (100.0 kV, 10.00 uA). The samples to be characterized were dispersed in ethanol through sonication and then dropped onto copper-grid-supported carbon films. The XRD patterns were recorded on Rigaku D/max-2500 X-ray diffractometer operated at 40 kV and 200 mA with Cu Kα (λ = 0.154 nm) radiation. The XPS measurements were carried out on the Thermo Scientific ESCALab 220i-XL at a pressure of about 5×10^{-9} mbar with 200W twinanode Al Kα radiation as the excitation source. The hydrocarbons C

1s line at 284.8 eV from adventitious carbon is used for energy referencing. The content of Pd and V in the catalyst was determined by ICP-AES (PROFILE. SPEC, Leeman). The X-ray absorption spectra including the X-ray absorption near-edge structure (XANES) and extended X-ray absorption fine structure (EXAFS) of the samples and references at Pd K-edge were recorded at BL14W1 beamline at Shanghai Synchrotron Radiation Facility (SSRF).

Computation details

All DFT calculations in this work were carried out using the Vienna Ab-initio Simulation Package (VASP)[1]. The projector augmented wave (PAW) method[2] and the Perdew-Burke-Ernzerhof (PBE) functional[3] utilizing the generalized gradient approximation (GGA)[4] were applied throughout the calculations. A large 9×9×9 and 8×8×8 K-point mesh[5] was first applied to Pd and PdO bulk structure for optimization, respectively.

A four-layer p (2×2) surface slabs for Pd (111), and four surface slabs for PdO were established in which (101) facet was considered as the most stable surface. A vacuum height of 15 Å was used to eliminate the interaction between neighbouring slabs. The Brillouin zone integration was performed using a 2×2×1 K-point mesh was used for PdO slab models, while a 3×3×1 K-point mesh was used for Pd (111) surfaces. The top two of all slabs were allowed to fully relax, while the bottom two layers were kept fixed to mimic the bulk region. The kinetic energy cut-off was set as 400 eV, the structure optimization force threshold was 0.05 eV/Å and the self-consistent calculations applied a convergence energy threshold of 10^{-5} eV. The transition states (TS) of surface reactions were located using CI-NEB[6] and dimer[7] methods. All TS were verified when (i) all forces on atoms vanish and (ii) the total energy is a maximum along the reaction coordination but a minimum with respect to the rest of the degrees of freedom. Vibrational analysis was carried out to ensure that the transition states have only one imaginary frequency along the reaction coordinate.

The catalytic reaction

The procedure was similar to our previous work[8]. The reaction was carried out in a 16 mL Teflon-lined stainless-steel autoclave with a magnetic stirrer. The pressure was determined by a pressure transducer (FOXBORO/ICT, Model 93) with ±0.025 MPa accuracy. In a typical experiment, a suitable amount of catalyst was added to base solution (1 M, 2 mL). The autoclave was sealed and purged with H_2 to remove the air at ambient temperature. Then H_2 and CO_2 were charged into the reactor to desired pressure in sequence. Next, the reactor was placed in a furnace of desired temperature and magnetic stirring was set at 700 rpm. After certain reaction time, the reactor was cooled down in ice water and the gas was released slowly and collected in a gas bag. The liquid mixture was analyzed via ^{1}H NMR (Bruker Avance III 400HD) in D_2O using dimethyl sulfoxide as the internal standard. The gaseous samples were analyzed using a GC (Agilent 4890D) equipped with a TCD detector and a packed column (Carbon molecular sieve TDX-01, 3 mm in diameter and 1 m in length) using Argon as the carry gas.

2. Supporting figures

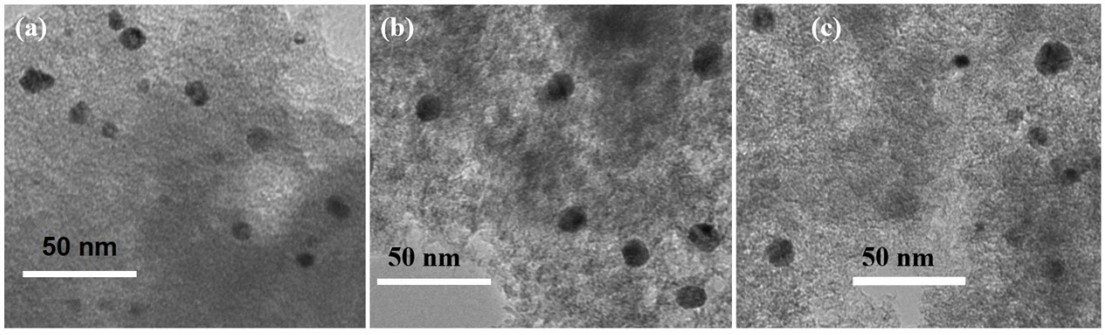

Fig S1. TEM image of (a) Pd/AC-air; (b) Pd/AC-H_2; (c) Pd-V/AC-H_2

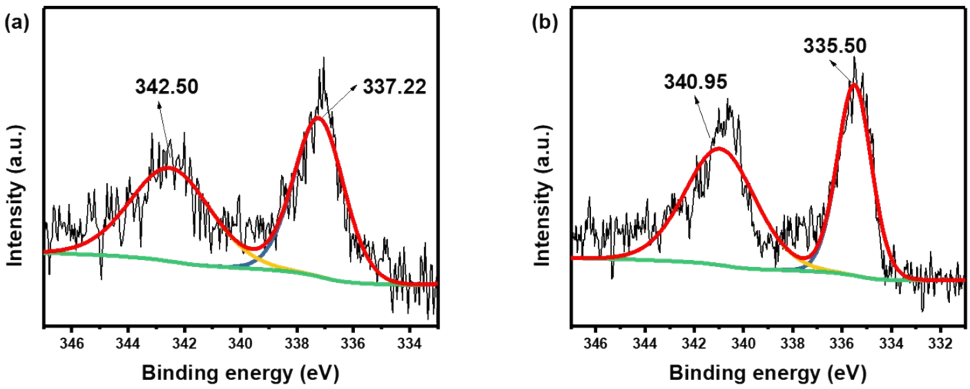

Figure S2. XPS spectra of Pd for (a) the Pd/AC-air catalyst and (b) the Pd/AC-H_2 catalyst.

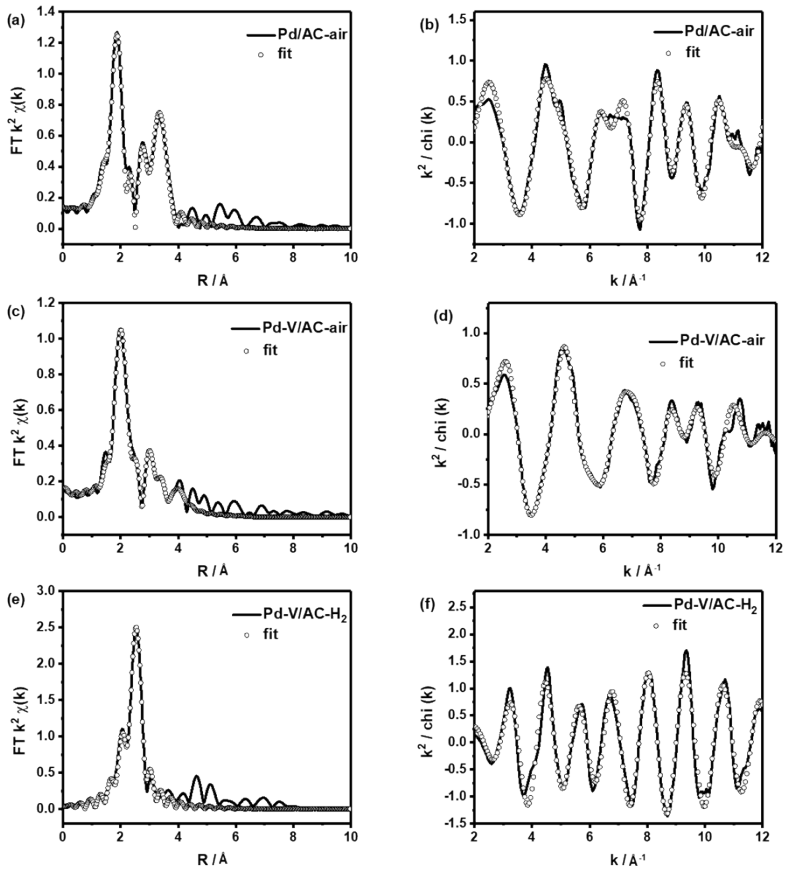

Fig S3. Fourier-transformed magnitude of Pd K-edge EXAFS spectra in R and k space for the prepared Pd/AC-air, Pd-V/AC-air and Pd-V/AC-H_2 catalysts.

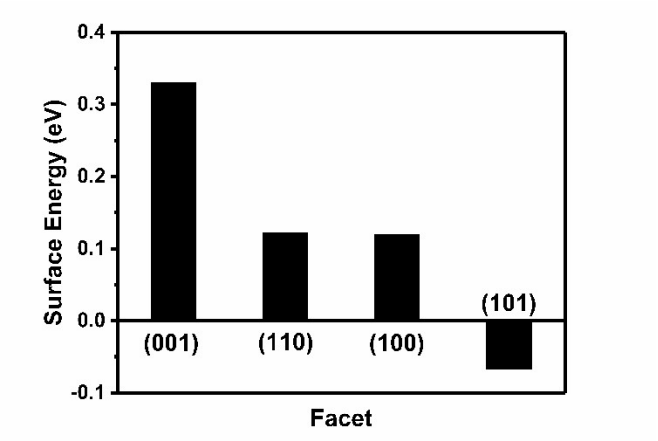

Figure S4. Surface energy of four possible PdO facets.

3. Supporting tables

Table S1. The catalytic performance for the hydrogenation of CO_2 to FA over reported heterogeneous catalysts.

Entry	Catalyst	Solvent	Base	P_{H2}/P_{CO2} (MPa)	T (K)	TON	TOF (h^{-1})	Reference
1	$PdMn_{0.6}$@S-1	H_2O	NaOH	2/2	353	-	2151	[9]
2	Pd@Ag/TiO_2	H_2O	$NaHCO_3$	1/1	373	2496	104	[10]
3	Pd/ZrO_2-T	H_2O	$NaHCO_3$	2/2	373	-	671	[11]
4	PdAg/amine-RF10	H_2O	$NaHCO_3$	1/1	373	867	36	[12]
5	PdAg/amine-MSC	H_2O	$NaHCO_3$	1/1	373	839	35	[13]
6	PdAg/SBA-15	H_2O	$NaHCO_3$	1/1	373	874	36	[14]
7	Pd/mpg-C_3N_4	D_2O	NEt_3	2.7/1.3	423	106	4.4	[15]
8	Pd/PIL-bipTf_2N	H_2O	NEt_3	2/2	373	1190	1190	[16]

Table S2. The effect of the additive base on the hydrogenation of CO_2 to formic acid.

Entry	base	TON
1	NaOH	2620
2	NEt_3	1453
3	$NaHCO_3$	3787
4	$KHCO_3$	3807
5	NH_4HCO_3	676
6	Na_2CO_3	4790
7	$CsCO_3$	450

Reaction conditions: Pd-V/AC-air (5 mg), base (1.0 M, 2 mL), P_{H2} (3 MPa), P_{CO2} (3 MPa), T (120°C), t (12 h).

Table S3. The effect of the gas pressure on the hydrogenation of CO_2 to formic acid.

Entry	P (H_2) (MPa)	P (CO_2) (MPa)	TON
1	1	5	2825
2	2	4	3480
3	3	3	4790
4	4	2	4818
5	5	1	4749
6	3	1	4790

Reaction conditions: Pd-V/AC-air (5 mg), Na_2CO_3 (1.0 M, 2 mL), T (120°C), t (12 h).

Table S4. The effect of various supports on the hydrogenation of CO_2 to formic acid.

Entry	catalyst	The theoretical Pd content (%)	Dosage (mg)	TON
1	Pd-V/a-TiO_2-air	3	50	141
2	Pd-V/P25-air	3	50	186
3	Pd-V/AC-air	3	50	203
4	Pd-V/SiO_2-air	1	30	25
5	Pd-V/com. SBA15-air	1	30	332
6	Pd-V/AC-air	1	30	1030
7	Pd-V/DMC-air	1	5	1515
8	Pd-V/AC-air	1	5	3787

Reaction conditions: $NaHCO_3$ (1.0 M, 2 mL), P_{H2} (3 MPa), P_{CO2} (3 MPa), T (120°C), t (12 h).

Table S5. The effect of reaction temperature on the hydrogenation of CO_2 to formic acid.

Entry	T (°C)	TON
1	80	1249
2	100	2682
3	120	4790
4	140	4503

Reaction conditions: Pd-V/AC-air (5 mg), Na_2CO_3 (1.0 M, 2 mL), P_{H2} (3 MPa), P_{CO2} (3 MPa), t (12 h).

Table S6. EXAFS parameters of the prepared catalysts as well as Pd foil and PdO standards.

Entry	Sample	Path	CN [a]	σ^2 (10^{-3} Å^2) [b]	ΔE_0 (eV) [c]	R (Å) [d]	R factor [e]
1	Pd foil	Pd-Pd	12*	5.45	2.914	2.739	0.006
2	PdO	Pd-O	4*	1.97	7.176	2.015	0.009
		Pd-O-Pd 1	4*	11.4	1.108	3.021	
		Pd-O-Pd 2	8*	14.7	1.108	3.366	
3	Pd/AC-air	Pd-O	3.83	2.64	6.505	2.005	0.019

		Pd-O-Pd 1	1.25	0.06	1.964	3.000	
		Pd-O-Pd 2	2.50	1.22	1.964	3.416	
4	Pd-V/AC-air	Pd-O	3.97	4.82	4.460	1.987	0.019
		Pd-O-Pd 1	1.69	5.28	2.078	3.056	
		Pd-O-Pd 2	1.69	10.8	2.078	3.365	
		Pd-O-V	3.43	10.8	12.76	3.653	
5	Pd-V/AC-H_2	Pd-Pd	10.63	6.44	1.195	2.738	0.007

The EXAFS data (k-range: 3.00 – 12.22 $Å^{-1}$ and R-range: 1 – 4 Å) were fitted in 1,2 and 3 k-weighted R-space. Amplitude reduction factors were evaluated for reference spectra.
a. CN: the coordination number; b. σ^2- Debye-Waller factor which measures thermal and static disorder in absorber-scattered distances; c.ΔE_0: edge-energy shift which means the difference between the zero kinetic energy value of the sample and that of the theoretical model; d. R: the interatomic distance (the bond length between central atoms and surrounding coordination atoms); e. R factor: the goodness of the fit. * means the coordination number of the standard samples are fixed.

Table S7. Energies of intermediates and transition states on Pd (111) and PdO (101). All energies are relative to the clean slab, CO_2 (g) and H_2 (g). "*" means that the intermediate is adsorbed on the surface.

Entry	Species	Energies of species (eV)	
		Pd (111)	PdO (101)
1	H_2*	-	-0.57
2	H_2* ⟶ H* + H* (TS)	-	-0.25
3	2 H* + CO_2	-1.50	-1.78
4	2 H* + CO_2 ⟶ HCOO* + H* (TS)	-0.02	-1.35
5	HCOO* + H*	-1.04	-2.32
6	HCOO* + H* ⟶ HCOOH* (TS)	-0.50	-0.97
7	HCOOH*	-0.97	-1.01
8	HCOOH (g)	-0.23	-0.23

Reference

[1] a) G. Kresse, J. Furthmuller, *Physical Review B* **1996**, *54*, 11169-11186; b) G. Kresse, J. Furthmuller, *Computational Materials Science* **1996**, *6*, 15-50; c) M. Hacene, A. Anciaux-Sedrakian, X. Rozanska, D. Klahr, T. Guignon, P. Fleurat-Lessard, *Journal of Computational Chemistry* **2012**, *33*, 2581-2589.
[2] P. E. Blochl, *Physical Review B* **1994**, *50*, 17953-17979.
[3] J. P. Perdew, K. Burke, M. Ernzerhof, *Physical Review Letters* **1997**, *78*, 1396-1396.
[4] M. P. Teter, M. C. Payne, D. C. Allan, *Physical Review B* **1989**, *40*, 12255-12263.
[5] H. J. Monkhorst, J. D. Pack, *Physical Review B* **1976**, *13*, 5188-5192.
[6] D. Sheppard, R. Terrell, G. Henkelman, *Journal of Chemical Physics* **2008**, *128*.
[7] P. Xiao, D. Sheppard, J. Rogal, G. Henkelman, *Journal of Chemical Physics* **2014**, *140*.
[8] a) Y. Wang, S. Li, Y. Yang, X. Shen, H. Liu, B. Han, *Chem. Commun.* **2019**, *55*, 6942-6945; b) Y. Wang, B. Chen, S. Liu, X. Shen, S. Li, Y. Yang, H. Liu, B. Han, *ChemCatChem* **2018**, *10*, 5124-5127.
[9] Q. Sun, B. W. J. Chen, N. Wang, Q. He, A. Chang, C. M. Yang, H. Asakura, T. Tanaka, M. J. Hulsey, C. H. Wang, J. Yu, N. Yan, *Angew. Chem. Int. Ed.* **2020**, *59*, 20183-20191.
[10] K. Mori, T. Sano, H. Kobayashi, H. Yamashita, *J. Am. Chem. Soc.* **2018**, *140*, 8902-8909.
[11] Z. Zhang, L. Zhang, M. J. Hülsey, N. Yan, *Molecular Catalysis* **2019**, *475*, 110461.
[12] S. Masuda, K. Mori, Y. Kuwahara, H. Yamashita, *J. Mater. Chem. A* **2019**, *7*, 16356-16363.
[13] S. Masuda, K. Mori, Y. Futamura, H. Yamashita, *ACS Catal.* **2018**, *8*, 2277-2285.
[14] K. Mori, S. Masuda, H. Tanaka, K. Yoshizawa, M. Che, H. Yamashita, *Chem. Commun.* **2017**, *53*, 4677-4680.
[15] J. H. Lee, J. Ryu, J. Y. Kim, S.-W. Nam, J. H. Han, T.-H. Lim, S. Gautam, K. H. Chae, C. W. Yoon, *J. Mater. Chem. A* **2014**, *2*, 9490.
[16] B. Feng, Z. Zhang, J. Wang, D. Yang, Q. Li, Y. Liu, H. Gai, T. Huang, H. Song, *Fuel* **2022**, *325*.